IEEE Robotics and Automation Letters (RA-L) paper, presented at ICRA 2026, Vienna, Austria. Cite as RA-L paper.

HADEC - High-Response Artificial Muscle Actuator using Dimethyl Ether Combustion

K. Mori[1], K. Tsurumi[1], R. Sawahashi[1], R. Enjo[1], T. Nakamura[1], *Member, IEEE,* and M. Okui[1], *Member, IEE*

***Abstract*—This paper introduces a high-response artificial muscle actuator using dimethyl ether combustion (HADEC), which is a novel method to enhance the responsiveness and force output of pneumatic actuators. The HADEC system integrates a McKibben-type artificial muscle filled with a combustible mixture of dimethyl ether (DME) and air, and it is ignited to generate rapid fluid pressure through combustion. This approach achieves force, displacement, and response speeds comparable to those of biological muscles while maintaining the simplicity and low-cost structure of McKibben-type actuators. The system provides instantaneous force generation without the need for complex mechanisms such as latches or brakes. DME, which is an environment- friendly fuel, ensures minimal emissions. Experimental results validate the effectiveness of HADEC in improving responsiveness, and the findings suggest superior force generation, faster response times, and high-frequency operability compared to that of conventional pneumatic actuators. Further, the paper discusses the potential for repeated actuation and highlights the benefits of HADEC in various robotic applications that require rapid and significant force.**

I. Introduction

SOFT robots have attracted considerable attention in robotics owing to their advantages such as their ability to perform motions that leverage their inherent flexibility, which enable them to emulate the superior movement principles of biological organisms as opposed to traditional actuators driven by electric motors and gear reducers [1-7]. Exisiting research focused on robots that mimic octopuses [1, 2] and those that achieve locomotion using soft bodies [3-7]. The key components of these flexible soft robots are their soft actuators. Given the objectives of soft robotics, it is desirable for these actuators to possess characteristics that are similar to those of biological muscles, including comparable contraction rates, contraction force, response speed, and variable stiffness. Consequently, numerous actuators were proposed [8-14], including shape memory alloys (SMA) [8, 9], dielectric elastomer actuators (DEA) [10, 11], HASEL actuators that drive fluids using DEA principles [12], and polymer artificial muscles [13, 14]. These technologies successfully harnessed the mechanical energy using various methods. However, a common problem with these actuators is insufficient force generation.

Manuscript received: December 13, 2024; Revised: April 22, 2025; Accepted: May 8, 2025.

This paper was recommended for publication by Editor Yong-Lae Park upon evaluation of the Associate Editor and Reviewers' comments.

This work was supported by JST, ACT-X Grant Number JPMJAX21K2, Japan.

1K. Mori, K. Tsurumi, R. Sawahashi, R. Enjo, T. Nakamura, and M. Okui are with the Faculty of Science and Engineering, Chuo University, Tokyo 112-8551, Japan (corresponding author: mokui147@g.chuo-u.ac.jp).

Digital Object Identifier (DOI): see top of this page.

Although most artificial muscle actuators successfully demonstrated a standalone operation, their individual force output was relatively low, and they failed to achieve significant force generation. Theoretically, these actuators generated stress levels equivalent to those of biological muscles (on the order of MPa), thereby achieving force amplification through integration. However, challenges related to increased failure rates and costs associated with integration have prevented successful scaling to the order of tens of Newtons, which is comparable to that of human muscles.

Fluid-driven actuators, such as pneumatic artificial muscles, stand out among soft actuators because of their ability to achieve contraction rates, contraction forces, and variable stiffness properties similar to those of human muscles. Their lightweight nature has led to the widespread use in assistive devices [15-18]. However, these devices fail to replicate the motions of living organisms, including humans. A major reason for this is the delay in response attributed to the compressibility of the working fluid in pneumatic systems, which results in a lower responsiveness compared to that of biological muscles. Existing research aimed at improving responsiveness such as work on controllers [20-22] is yet to address the structural limitations of response frequency. Other methods, such as those that utilize artificial muscles with magnetorheological fluids [23] and those combining magnetic brakes with pneumatic cylinders [24], can enable rapid movements by instantaneously releasing stored elastic energy. However, these involve multiple processes and do not fundamentally improve the responsiveness of the actuator. Although there are examples of actuators driven by hydraulic or hydrostatic pressures [25, 26], these compromises the flexibility afforded by the compressibility of air.

Therefore, we introduced a high-response artificial muscle actuator using dimethyl ether combustion (HADEC). This method involves filling a McKibben-type artificial muscle [27, 28], which is a representative fluid-driven actuator with dimethyl ether (DME), igniting it, and generating fluid pressure through the thermal energy produced by combustion. This approach achieves force, displacement, and response speeds comparable to those of biological muscles while maintaining the structural simplicity of McKibben-type artificial muscles, thereby making it suitable for industrial production. In addition, this system can function as a conventional compressed gas-driven actuator using the same configuration as that for combustion-driven actuation. This method offers a simpler implementation than existing methods that use latches or brakes because instantaneous force can be generated without preparatory actions as long as the gas is pressurized.

IEEE Robotics and Automation Letters (RA-L) paper, presented at ICRA 2026, Vienna, Austria. Cite as RA-L paper.

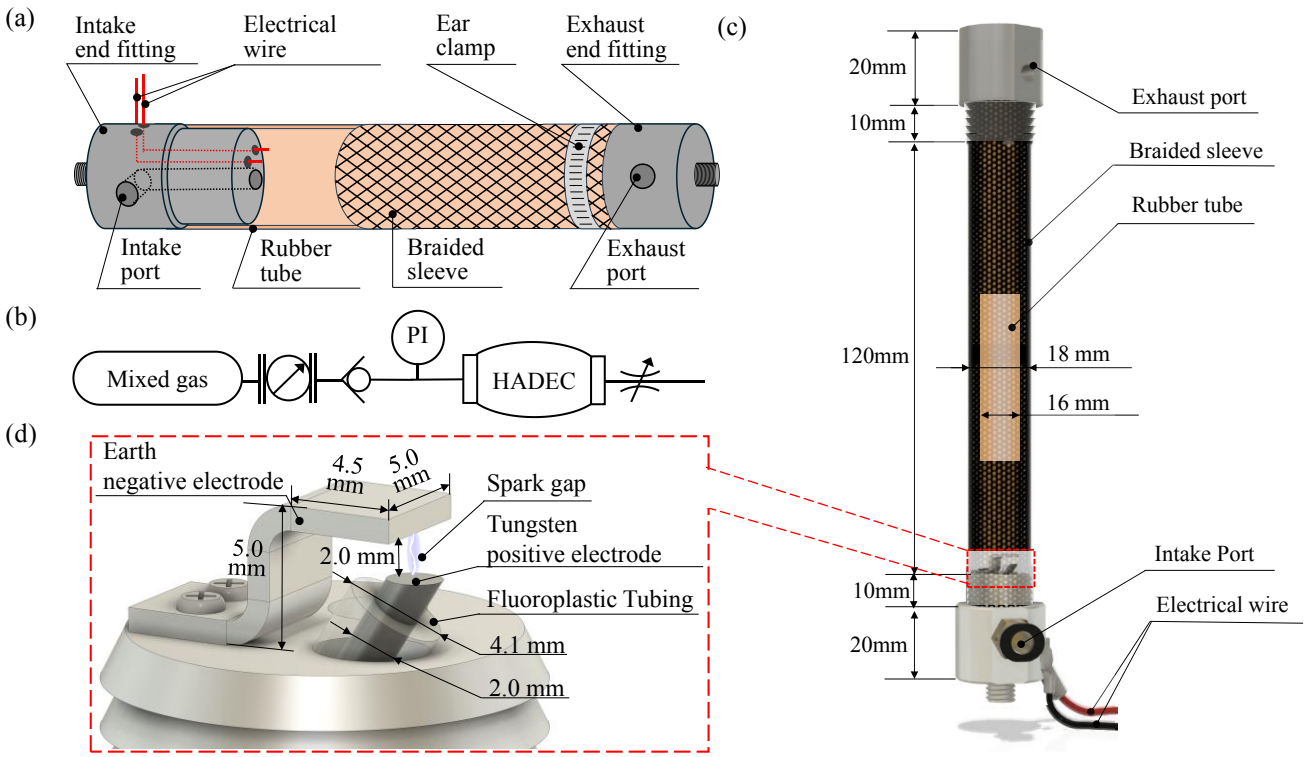

Fig. 1 HADEC Overview: (a) Drive concept. DME is supplied and exhausted from end fittings on the left and right sides. Combustion can be performed by using an ignition device on the intake end fitting. (b) Pneumatic circuit. A speed controller is used on the exhaust side to adjust the flow rate on the exhaust side. (c) Prototype. The ignition device sends high voltage from a wire to ignite the ignition.(d) Ignition part, electrode.

Although there are previous examples of combustion-driven robots [29], they have been limited to applications such as jumping. The proposed method is novel because of its potential for use as a general-purpose linear actuator. This paper presents the application of a DME combustion-based responsiveness improvement method for a robotic system and validates its effectiveness through experimental verification.

II. Overview of the HADEC

A. Principle

Fig. 1 presents an overview of a HADEC, which features an ignition device (d) inside a McKibben-type artificial muscle (a). The McKibben-type artificial muscle comprises a cylindrical rubber tube wrapped in a mesh sleeve. The rubber tube expanded when air pressure was applied inside the artificial muscle, which changed the angle of the fibers and generated an axial force. In HADEC, a McKibben-type artificial muscle is filled with a combustible mixture of DME and air, and ignition is initiated by the ignition device. Consequently, a rapid increase in pressure caused by the combustion of the gas mixture is used to drive the artificial muscle. Further, the HADEC can function as a conventional McKibben-type artificial muscle by applying internal pressure.

DME, the fuel used for combustion, is an oxygenated fuel that does not produce soot because it lacks carbon–carbon bonds [30]. In addition, they emit extremely low levels of particulates, which are a major cause of air pollution, thereby making them promising candidate fuels for next-generation clean diesel engines. Although DME is a gas at room temperature and pressure, it liquefies when pressurized to 0.53 MPa at 20 °C, making it easy to store in liquefied form. This characteristic enables it to be carried in a lightweight and inexpensive aluminum can in liquid form at room temperature. During mass production, a 480-ml can contains 231 g of DME. To drive the artificial muscle shown in Fig. 1(c), ~5 mg of DME was required, thereby allowing the aforementioned commercial can to facilitate ~46,000 actuations.

B. Design

Fig. 1(c) shows a prototype HADEC comprising an ignition device, rubber tube, sleeve, and crimp parts. The ignition device had a tungsten electrode with a tungsten rod attached as the anode, and a ground (GND) electrode attached to an aluminum component, as shown in Fig. 1(d). A tungsten rod and cathode plate were designed for maintaining 2mm gap. Then, the sleeve was covered with a rubber tube and attached to an end-fitting with an ignition device. The end fitting, rubber tube, and sleeve were secured using crimps. The other side was secured similarly to the end fitting without the igniter. The materials used are simple and cost-effective. The rubber tubing and braided sleeves are available for only a few dollars, and the aluminum end fittings are priced at approximately $50 for this prototype. Thus, HADEC was produced at a low cost.

Additionally, the HADEC's igniter has undergone repeated driving tests and has been confirmed to operate stably even after 50,000 cycles. While we have not conducted lifetime evaluation of the assembled HADEC, this prototype has been driven over 1000 cycles during experimental evaluations, and it continues to function without issues.

III. Modeling

We modeled the internal pressure and isometric contraction force during the combustion of the HADEC. Fig.

IEEE Robotics and Automation Letters (RA-L) paper, presented at ICRA 2026, Vienna, Austria. Cite as RA-L paper.

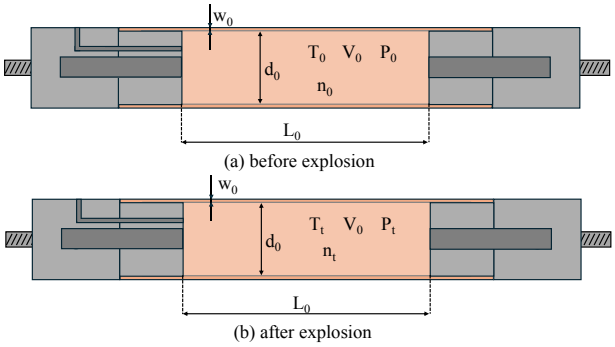

Fig. 2 Model of artificial muscle driven by combustion. End fittings are attached on the left and right sides, and can be fixed to the parts by means of screws. The holes in the center are for DME supply and exhaust. Parameters are listed at the end. (a) Parameters before combustion. (b) Parameters after combustion.

2 shows the model, and Table III lists the parameters. In the model, all gases were assumed to be ideal gases, and the initial state of the artificial muscle was cylindrical. A mixture of DME and air, pre-mixed at an air-fuel ratio r, was assumed to be uniformly distributed inside the artificial muscle at a pressure of P_0 . In this case, the total heat quantity Q_{in} generated via combustion is given by

$$Q_{in} = \frac{rMP_0V_0Q_{dme}}{RT_0}. \quad (1)$$

The volume V_0 of the artificial muscle is expressed by

$$V_0 = \frac{\pi d_0^2 L_0}{4}. \quad (2)$$

Subsequently, the combustion time was considered. Burning begins at one end of the artificial muscle where the sparker is located and is completed when it reaches the other end. Using the DME burning propagation velocity v_{dme}, the burning time t_{dme} can be calculated as

$$t_{dme} = \frac{L_0}{v_{dme}}. \quad (3)$$

Thus, the heat per hour q generated by combustion can be expressed as an impulse input

$$q = \begin{cases} \frac{Q_{in}}{t_{dme}} & (0 \le t \le t_{dme}) \\ 0 & (t_{dme} \le t) \end{cases}. \quad (4)$$

Then, if the temperature inside the artificial muscle is T_t, the temperature variation with $\Delta t[s]$ is given by

$$T_{t+\Delta t} = T_t + \frac{(q - q_{out})\Delta t}{n_0 c_v + C}. \quad (5)$$

In this study, q_{out} represents the amount of heat released from the artificial muscle into the atmosphere and is expressed as

$$q_{out} = \frac{S\lambda(T_t - T_0)}{w_0}. \quad (6)$$

The number of moles of gas inside the artificial muscle n_t is given by

$$n_t = \begin{cases} n_0\left(1 + \frac{rt}{t_{dme}}\right) & (0 \le t \le t_{dme}) \\ n_0(1+r) & (t_{dme} \le t) \end{cases}. \quad (7)$$

From (7), pressure P_t can be obtained using the Boyle-Charles law

$$P_t = \frac{n_t R T_t}{V_0}. \quad (8)$$

The isometric contraction force F_t of the artificial muscle can be calculated using the McKibben-type pneumatic artificial muscle contraction force model using [31, 32]

$$F_t = \frac{\pi d_0^2 P_t}{4\sin^2\theta_0}\{3(1-\varepsilon_0)^2\cos^2\theta_0 - 1\}. \quad (9)$$

IV. Basic Characteristic Experiments

A. Experimental setup

We conducted basic experiments on the forces and displacements of the HADEC and compared them with the model presented in Section 3. The experimental setup is shown in Fig. 3. The testing machine can fix one end of the HADEC and the other end using a slider. This slider can be fixed to limit displacement in isometric tests. In the displacement measurement tests, the slider was moved freely to measure the displacement response. In the experiment, the ignition device generated sparks inside the artificial muscle that ignited the gas mixture. The pressure at the time of combustion of the gas mixture was measured using a pressure gauge (SMC PSE540); the contraction force of the artificial muscle was measured using a load cell (KYOWA LUX-B-ID); and the displacement of the reflector attached to the slide rail was measured using a laser displacement meter (Panasonic HG-C1200). A mixture of DME and air was mixed in advance and allowed to remain inside the artificial muscle. The mixing ratio of this gas mixture was the ratio (DME molar ratio of 7%) at which the pressure increase because the combustion is the largest in a preliminary experiment [33]. The speed controller shown in Fig. 3 was completely closed at the time of ignition to prevent gas leakage. The inner diameters of the artificial muscles were 12 mm, and the experiments were conducted in triplicates.

In addition to the experimental conditions described above, the pressure of the mixed gas before ignition was included as an experimental parameter. For the isometric force characteristic experiment, five experimental conditions were set by varying the applied pressure of the gas mixture to 0, 10, 20, 30and 40 kPa. For the 0 kPa condition, the gas mixture was filled into the artificial muscle and exhausted to create the baseline state. In the contraction characteristic experiment, a 40 kPa condition was added, and four conditions were prepared in total.

For the force characteristics experiment, a comparison was drawn between the pressure and force calculated using the model described in Section 3. The parameters used for comparison are listed in Table III. The flame propagation speed was determined based on the results of the flame propagation test presented in the Appendix. Parameters C and θ_0 were identified from the experimental results.

IEEE Robotics and Automation Letters (RA-L) paper, presented at ICRA 2026, Vienna, Austria. Cite as RA-L paper.

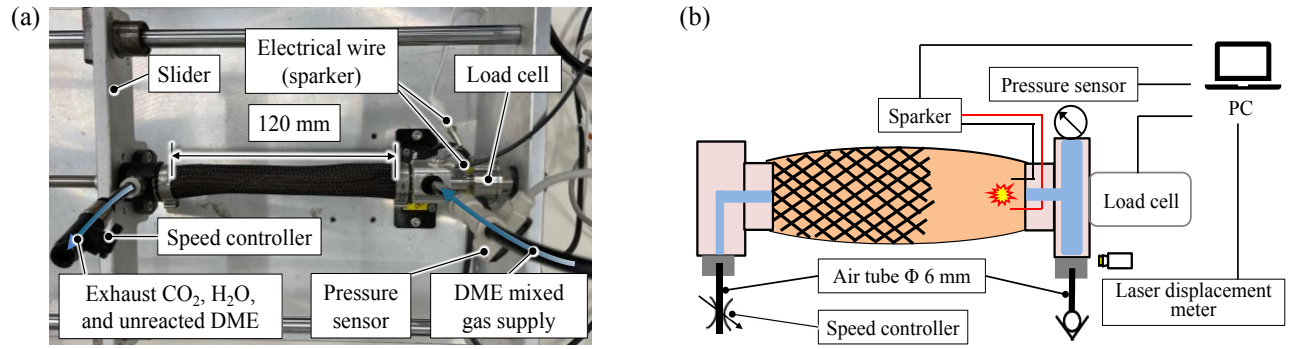

Fig. 3 Experimental environment: (a) Actual experimental setup and (b) equipment overview.

TABLE I. PRESSURE AND GENERATED FORCE

P [kPa]	Dead time [ms] (Pressure)		Dead time [ms] (Force)		Peak time [ms]	
0	1.95	±0.653	4.28	±0.179	45.9	±4.02
10	1.42	±0.722	3.05	±0.237	42.3	±0.693
20	1.78	±0.776	3.17	±0.141	43.0	±0.414
30	1.28	±0.251	2.98	±0.0854	37.6	±2.11

TABLE II. PRESSURE AND DISPLACEMENT

P [kPa]	Dead time [ms] (Pressure)		Dead time [ms] (Displacement)		Peak time[ms] (Displacement)	
0	1.52	±0.894	12.3	±0.624	87.1	±3.42
10	1.12	±0.125	9.66	±1.06	53.9	±0.584
20	1.26	±0.100	8.58	±0.210	46.9	±0.402
30	1.81	±0.241	10.1	±0.721	34.2	±3.38
40	1.64	±0.276	9.07	±0.525	48.2	±1.06

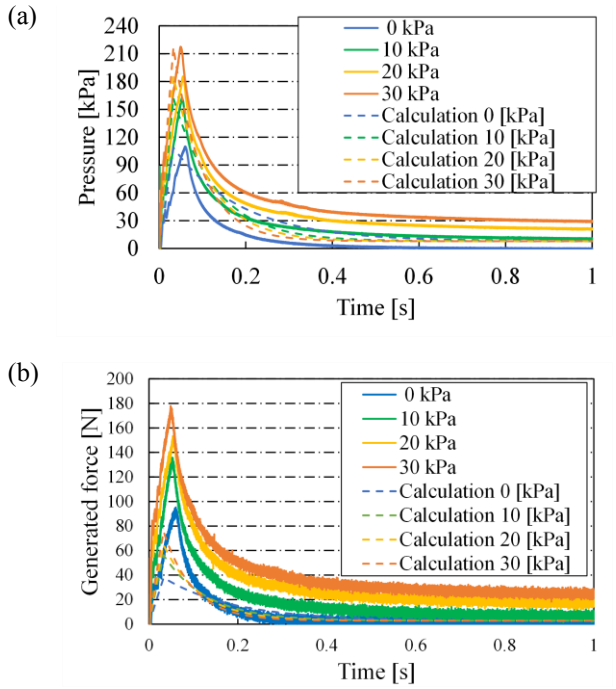

Fig. 4 Results of force response experiments: (a) Measured pressure response in the actuator in the force response experiment. (b) Measured generated force response.

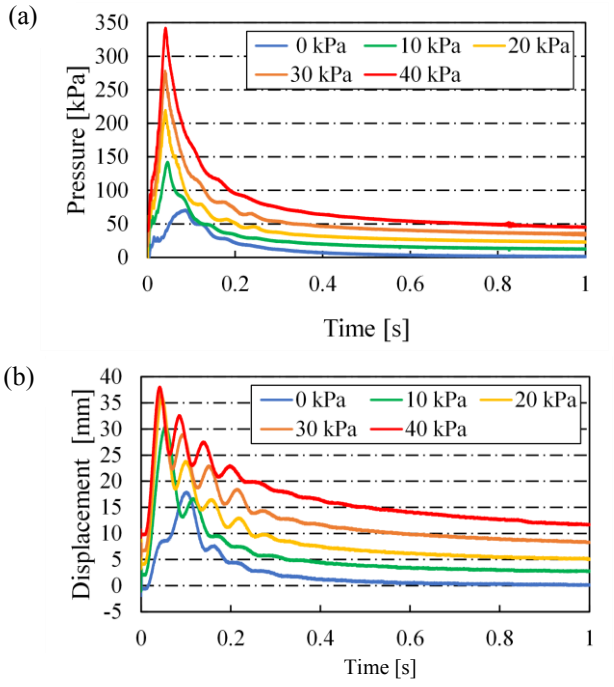

Fig. 5 Results of displacement response experiments: (a) Measured pressure response in the actuator in the displacement response experiment. (b) Measured displacement response.

B. *Force characteristics*

The experimental results are presented in Table I and Fig 4. The experimental results confirmed that the DME combustion-driven artificial muscle exhibited a high force response at all pressures. Conventional pneumatic systems, including pneumatic artificial muscles, typically experience a dead time of tens of milliseconds to 100ms, along with delays in force and displacement responses [34, 35]. A comparison of the dead time and peak time with conventional pneumatic artificial muscles showed that the proposed method had a superior response speed.

The experimental results were in close agreement with the theoretical values with respect to the internal pressure in the graph. The trends of the theoretical and experimental values for the shrinkage force were in good agreement. However,

IEEE Robotics and Automation Letters (RA-L) paper, presented at ICRA 2026, Vienna, Austria. Cite as RA-L paper.

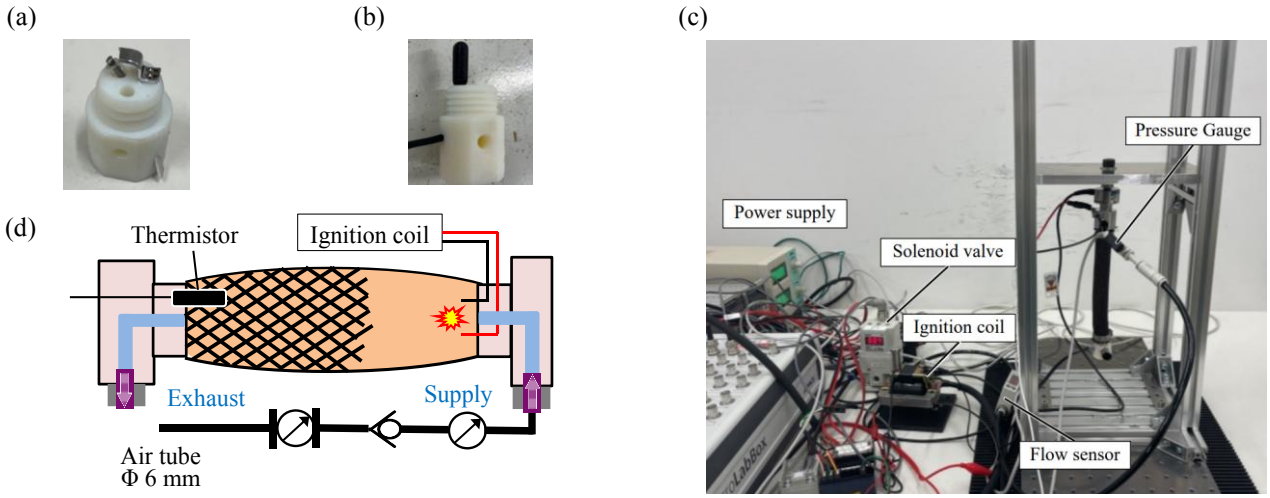

Fig. 6 Experimental setup: (a) Intake-side end fitting, (b) exhaust-side end fitting, (c) experimental apparatus, and (d) equipment overview.

discrepancies were observed between the simulation and experimental results in terms of both the peak value and the time to reach the peak. The deviation in the peak value is attributed to the variation in the initial braiding angle of the braided sleeve at different locations, making accurate measurement challenging. This measurement uncertainty is considered to be the primary cause of the discrepancy. On the other hand, the deviation in the time to reach the peak is likely due to the failure to account for the time delay in the process of converting pressure into force. In practice, as the pressure increases, the Ame rubber tube first expands, and subsequently, the braided sleeve is tensioned, generating force. However, in the simulation, the transmission delay between the occurrence of a pressure change and the generation of force was not considered. This omission is believed to be the cause of the observed time discrepancy.

We believe that this method can be adapted for applications that require sudden and large forces by adjusting the applied pressure according to the intended use of the artificial muscle.

C. Contraction (Displacement) characteristics

The experimental results are presented in Table II and Fig 5. At all applied pressures, the DME combustion-driven artificial muscle exhibited a minimum dead time of few milliseconds and a high displacement response. Furthermore, the time to reach the maximum internal pressure (peak time) was ~50 ms, which indicates high-pressure responsiveness. These results suggest that the proposed method effectively improved the responsiveness of pneumatic actuation systems, which typically have a dead time of tens of milliseconds to 100ms and delays in displacement responses[34, 35].

V. Repeated Actuation of the HADEC

Once the HADEC was driven, it was necessary to exhaust the gas after the reaction and refill it with a mixture of DME and air. Using a prototype, we verified the number of operating cycles that could be repeatedly driven.

A. Experimental environment

Fig. 6 shows the experimental environment. A thermistor (SEMITEC 103AT-11) is attached to the exhaust. In the experiment, the interior of the artificial muscle was filled in advance with a continuously flowing mixture of DME and air. On the exhaust side, the mixed gas was discharged at a fixed rate using a speed controller. The mixing ratio of the mixed gas was set to the ratio (DME molar ratio of 7%) at which the pressure increased due to the combustion being the highest in the preliminary experiment. A high voltage was generated using an ignition coil (Kitako, Model B), and a spark was generated using an ignition device inside the artificial muscle to burn the gas mixture. The gas mixture always flowed so that it could be ignited at any time. The inner diameter of the artificial muscle was 16 mm. The pressure during combustion was measured using a pressure gauge (PISCO, SEU11-6UA), and the flow into the artificial muscle was measured using a flow meter (SMC, PFM750-C6-C-M). The room temperature was 25 °C and the humidity was 44%.

B. Experimental procedure

The air supply side of the artificial muscle was set at the fixed end and the exhaust side at the free end, and the air flow continued without blocking the exhaust port. The flow rate was fixed at 13.0 L/min. The experimental conditions were three patterns with spark-ignition frequencies of 1, 5, and 10 Hz, respectively. In the preliminary experiment, ignition at a frequency of 20 Hz failed to activate the HADEC properly. Therefore, we concluded that the DME combustion-driven artificial muscle could be driven stably up to 10 Hz at a flow rate of 13.0 L/min, and we set the experimental conditions to frequencies of 1, 5, and 10 Hz. For all conditions, continuous operation was conducted until the measured internal temperature exceeded 80°C. After that, the system was left idle for 15 seconds, and before reuse, the experiment was performed only after the temperature had dropped back to room temperature (25°C).

C. Experimental results

Fig. 7 (a) shows the time variation of the temperature rise for each condition, and Fig. 7 (b) shows the time elapsed until the measured internal temperature reached 80 °C. Fig. 7 (c)–(e) show the response of the internal pressure during the first

IEEE Robotics and Automation Letters (RA-L) paper, presented at ICRA 2026, Vienna, Austria. Cite as RA-L paper.

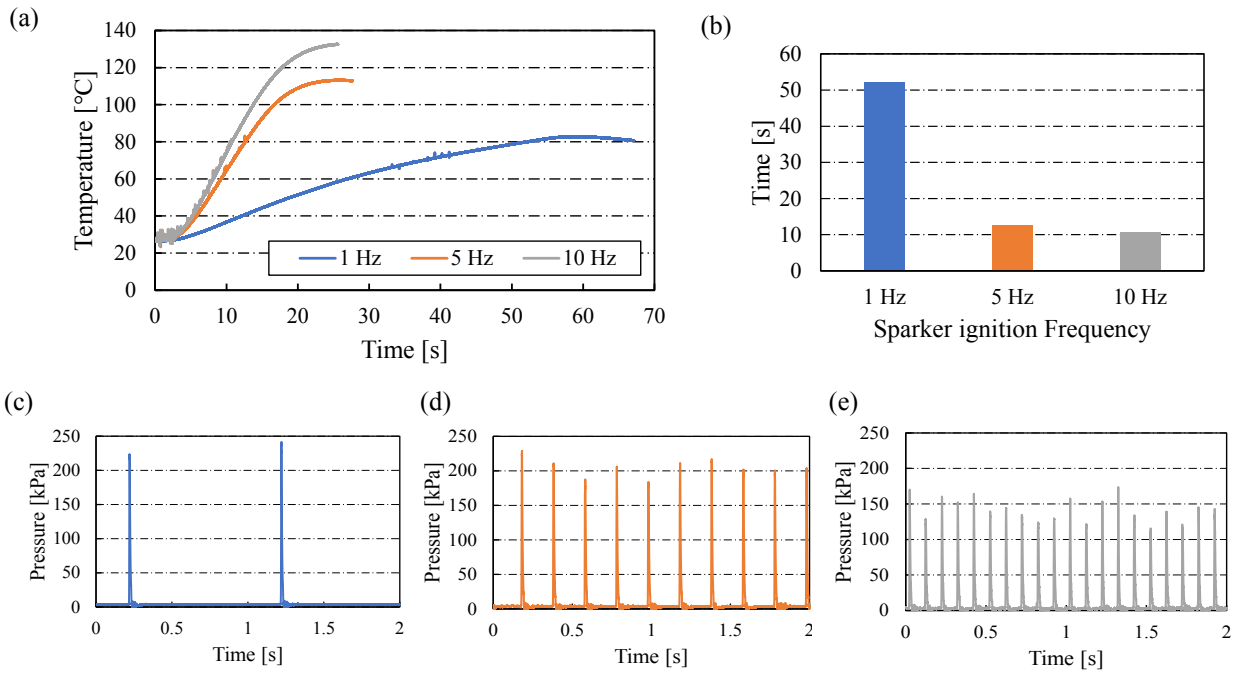

Fig. 7 Experimental environment of chapter V. (a) Temperature rises for each sparker ignition frequency. (b) Elapsed time until the measured internal temperature reaches 80°. (c)–(e) Internal pressure response (1, 5, and 10 Hz) of the repeated drive experiment.

2 s, i.e., from 5 to 7 s after the start of the experiment. Figs. 7 (c)–(e) show that the internal pressure increased at a frequency equivalent to the ignition frequency under all conditions. However, as shown in Figure 7(a), the temperature rose significantly under the 10-Hz condition, exceeding the heat resistance limit of 120°C for natural rubber, and reached 80°C within 10 seconds of the start of the experiment, as shown in Figure 7(b). Therefore, considering the use of a heat-resistant rubber or cooling outside the artificial muscle, such as in water, is necessary to drive an artificial muscle at a high frequency within a safe range. In Figs. 7(c) and 7(e), the peak pressure was 200 kPa for the 1 Hz drive, whereas it was ~150 kPa for the 10 Hz drive. This can be attributed to the gas mixture after the combustion is not exhausted sufficiently before the next combustion. We confirmed that the proposed artificial muscle could be driven repeatedly and that the drive frequency could be varied according to the ignition frequency of the ignition device.

VI. Conclusion

We developed an instantaneous force generator using DME combustion-driven artificial muscles named HADEC. The HADEC has the following advantages over conventional artificial muscle actuators: lower cost, simpler configuration, faster response, and force generation compared to conventional artificial muscle actuators. In addition, HADECs can be driven with a low-cost and simple configuration compared with conventional artificial muscle actuators because the DME consumed per actuation is small. Leveraging its characteristics, HADEC can be applied in various fields, including assistive care robots, collaborative robots, and as an alternative for percussion inspection at construction sites.

As part of our future plans, we will conduct experiments to investigate the characteristics such as peak pressure at different operating frequencies and the supply pressure and molar concentration of mixed gas to further clarify actuator characteristics. In addition, to clarify the actuator's positioning, we will develop equipment capable of measuring output power and use it to define its positioning, as well as assess thermal efficiency and other factors.

Appendix: Observation of Flame Propagation

The combustion time of DME in the model was expressed based on the combustion rate. However, the fundamental characteristics of the DME combustion speed are not well understood. Although related studies have focused on the factors affecting the combustion rate and its application to engines, an understanding of the fundamental combustion characteristics of DME remains insufficient [36-40]. Therefore, the objective of this study is to clarify the unexplored combustion rate characteristics. In the experiment, a HADEC was created using a transparent silicon tube with a length of 100 mm and an inner diameter of 16 mm, without an attached sleeve to allow for observation of the interior. The process from ignition to the end of the combustion was recorded using a high-speed camera at 240 fps to document the combustion in detail.

The results of the experiment are shown in Fig. 8 Immediately after ignition, the flame propagated to about half of the tube in 4.1 ms, after which the speed decreased and reached the end in about 33.3 ms. Thereafter, combustion at the end lasted ~30 ms. Based on these results, it was assumed that combustion occurred during the time until the flame reached the end, and the combustion lasted for 33.3 ms in the 100 mm tube. In other words, the combustion time

IEEE Robotics and Automation Letters (RA-L) paper, presented at ICRA 2026, Vienna, Austria. Cite as RA-L paper.

was assumed to be 40 ms because a 120 mm long HADEC was used in the force-measurement experiment.

REFERENCES

[1] J. Fras, Y. Noh, M. Macias, H. Wurdemann, and K. Althoefer, "Bio-Inspired Octopus Robot Based on Novel Soft Fluidic Actuator," in *ICRA*, Brisbane, QLD, Australia, 2018, pp. 1583–1588.

[2] Y. Hotoda and K. Ito, "Octopus-like soft robot hand for handling vegetables and fruits," in *ICAMechS*, Melbourne, Australia, 2023, pp. 13–18.

[3] R. Chen, X. Zhu, Z. Yuan, H. Pu, J. Luo, and Y. Sun, "A bioinspired single actuator-driven soft robot capable of multistrategy locomotion," *IEEE Trans. Robot.*, vol. 40, pp. 2149–2165, 2024.

[4] J. Tirado, J. Jørgensen, and A. Rafsanjani, "Earthworm-inspired multimodal soft actuators," in *RoboSoft*, Singapore, Singapore, 2023, pp. 1–6.

[5] D. D. K. Arachchige, D. M. Perera, S. Mallikarachchi, U. Huzaifa, I. Kanj, and I. S. Godage, "Soft steps: Exploring quadrupedal locomotion with modular soft robots," *IEEE Access*, vol. 11, pp. 63136–63148, 2023.

[6] X. Ai, H. Yue, and W. D. Wang, "Crawling soft robot exploiting wheel-legs and multimodal locomotion for high terrestrial maneuverability," *IEEE Trans. Robot.*, vol. 39, no. 6, pp. 4230–4239, Dec. 2023.

[7] W. R. Johnson, S. J. Woodman, and R. Kramer-Bottiglio, "An electromagnetic soft robot that carries its own magnet," in *RoboSoft*, Edinburgh, United Kingdom, 2022, pp. 761–766

[8] M. Liu and L. Hao, "Design and control of a robotic wrist joint actuated by the shape memory alloy actuator," in *CYBER*, Jiaxing, China, 2021, pp. 225–229.

[9] H. F. M. Ali, and Y. Kim, "Novel bio-inspired artificial muscle using shape memory alloy wire in spiral winding," in *ICCAS*, Yeosu, Korea, Republic of, 2023, pp. 1169–1173

[10] A. Walter, T. Martinez, Y. Civet, and Y. Perriard, "Study of the use of silver trace and improved flexibility in rolled Dielectric Elastomer Actuators," in *ICEMS*, Chiang Mai, Thailand, 2022, pp. 1–6

[11] M. Kadokawa and C. Jiang, "Development of a thin dielectric elastomer actuator with 3DOFs," in *ICAMechS*, Tokyo, Japan, 2021, pp. 12–15

[12] Y. Yeh, N. Cisneros, Y. Wu, K. Rabenorosoa, and Y. L. Gorrec, "Modeling and position control of the HASEL actuator via Port-Hamiltonian approach," *IEEE Robot. Automat. Lett.*, vol. 7, no. 3, pp. 7100–7107, July 2022

[13] S. Terryn, J. Brancart, D. Lefeber, G. Van Assche, and B. Vanderborght, "A pneumatic artificial muscle manufactured out of self-healing polymers that can repair macroscopic damages," *IEEE Robot. Automat. Lett.*, vol. 3, no. 1, pp. 16–21, Jan. 2018

[14] F. Karami, L. Wu, and Y. Tadesse, "Modeling of one-ply and two-ply twisted and coiled polymer artificial muscles," *IEEE/ASME Trans. Mechatron.*, vol. 26, no. 1, pp. 300–310

[15] Y. Hashimoto, Y. Nakanishi, N. Saga, J. -Y. Nagase, and T. Satoh, "Development of gait assistive device using pneumatic artificial muscle," in *SCIS and ISIS*, Sapporo, Japan, 2016, pp. 710–713

[16] K. Tripanpitak, T. V. J. Tarvainen, I. Sönmezisik, J. Wu, and W. Yu, "Design a soft assistive device for elbow movement training in peripheral nerve injuries," in *ROBIO*, Macau, Macao, 2017, pp. 544–548

[17] M. Ide, T. Hashimoto, K. Matsumoto, and H. Kobayashi, "Evaluation of the power assist effect of muscle suit for lower back support," *IEEE Access*, vol. 9, pp. 3249–3260, 2021.

[18] W. D. Doyle, "Magnetization reversal in films with biaxial anisotropy," in *1987 Proc. INTERMAG Conf.*, pp. 2.2-1–2.2-6.

[19] T. Abe, S. Koizumi, H. Nabae, G. Endo, and K. Suzumori, "Muscle textile to implement soft suit to shift balancing posture of the body," in *RoboSoft*, Livorno, Italy, 2018, pp. 572–578

[20] H. Fu, Y. Liu, and J. Chen, "Bio-inspired modeling and position control for pneumatic artificial muscle," in *YAC*, Zhanjiang, China, 2020, pp. 697–701

[21] R. Kako, N. Saito, D. Furukawa, and T. Satoh, "Muscle activity control using an EMG feedback based pneumatic artificial muscle power-assist device," in *IECON*, Singapore, 2020, pp. 644–649.

[22] S. P. Bingulac, "On the compatibility of adaptive controllers," in *Proc. 4th Annu. Allerton Conf. Circuits and Systems Theory*, New York, 1994, pp. 8–16.

[23] T. Nagayama, H. Ishihara, H. Tomori and T. Nakamura, "Throwing operations by manipulator with a 2-DOF variable viscoelastic joint using pneumatic artificial muscles and a magnetorheological brake," in *ROBIO*, Zhuhai, China, 2015, pp. 2324–2329

[24] M. Cinq-Mars and H. Gurocak, "Pneumatic actuator with embedded MR-brake for haptics," in *WHC*, Munich, Germany, 2017, pp. 322–327

[25] Y. Feng *et al*., "Experimental validation of a 7-DOF power soft robot driven by hydraulic artificial muscles," *IEEE Robot. Automat. Lett.,* vol. 9, no. 6, pp. 5472–5479, June 2024

[26] C. Jin-kai et al., "Design and experiment of a water hydraulic artificial muscle actuated diving auxiliary operating system," in *FPM*, Lanzhou, China, 2023, pp. 1–7

[27] J. Kadowaki, D. Sasaki, H. Yase, and R. Kusaka, "Improvement of McKibben type artificial rubber muscle model based on end shape deformation," in *ICM*, Kashiwa, Japan, 2021, pp. 1–6

[28] M. A. Khan, S. Shaik, M. H. Tariq, and T. Kamal, "McKibben pneumatic artificial muscle robot actuators - A review," in *ICRAI*, Peshawar, Pakistan, 2023, pp. 1–6

[29] N. W. Bartlett, M. T. Tolley, J. T. B. Overvelde, J. C. Weaver, B. Mosadegh, K. Bertoldi, G. M. Whitesides, R. J. Wood, "A 3D-printed, functionally graded soft robot powered by combustion," *Science* vol. 349, pp. 161–165, 2015.

[30] T. Kaoru, "Dimethyl ether (DME): a clean fuel/energy for the 21st century and the low carbon society," *Int. J. Energy Environ*., vol. 10, pp. 248–252, 2016.

[31] A. Nozaki and T. Noritsugu, "Finite element analysis of the motion of McKibben-type pneumatic rubber artificial muscles," *Int. J. Automat. Technol.*, vol. 8, no. 2, p. 147–158, 2014. Published online: 2019/07/01, Online ISSN 1883-8022, Print ISSN 1881-7629

[32] Chou, C. P., & Hannaford, B. (1996). Measurement and modeling of McKibben pneumatic artificial Muscles. IEEE Transactions on Robotics and Automation, 12(1), 90-102.

[33] R. Enjo, M. Okui, and T. Nakamura, "Pneumatic source proposal for improving portability and responsiveness of artificial muscle via dimethyl ether phase change and combustion," in *Proc. 11th JFPS Int. Symp. on Fluid Power*, pp. 169–174.

[34] Y. Yamada, A. Kojima, M. Okui, Y. Higashi, T. Nakamura, "Hollow Pneumatic Artificial Muscles with Air Cylinder： Improvement for Compatibility of High Durability and High Efficiency", *7th IEEE International Conference on Biomedical Robotics and Biomechatronics (Biorob)*, 2018, pp. 865-870

[35] K. N. Kamaludin, L. Abdullah, S. N. S. Salim, Z. Jamaludin, M. N. Maslan and M. F. Rahmat, "Comparison of a Double and Triple Nonlinear Hyperbolic Proportional-Integral-Derivative (PID) compensator for a servo pneumatic actuator," *13th Asian Control Conference (ASCC)*, Jeju, Korea, Republic of, 2022, pp. 1775-1781,

[36] Z. Huang, Q. Wang, J. Yu, Y. Zhang, K. Zeng, H. Miao, and D. Jiang, "Measurement of laminar burning velocity of dimethyl ether–air premixed mixtures," *Fuel*, vol. 86, no. 15, pp. 2360–2366, 2007.

[37] W.P. Fan, Y. Gao, Y.M. Zhang, et al., "Numerical studies on turbulent flame propagation in premixed gas deflagration inside a tube," *Build. Simul*. vol. 13, pp. 849–864, 2020.

[38] H.W. Wang, Z.H. Huang, L.B. Zhou, D.M. Jiang, and Z.L. Yang, "Investigation on emission characteristics of a compression ignition engine with oxygenated fuels and exhaust gas recirculation," in *Proc. Inst. Mech. Eng. D: J. Automobile Eng.* vol. 214, no. 5, pp. 503–508, 2000.

[39] F. Maroteaux, G. Descombes, F. Sauton, and J. Jullien, "Investigation on exhaust emissions of a common rail high-speed direct injection diesel engine running with dimethyl ether," *Int. J. Engine Res.,* vol. 2, no. 3, pp. 199-207, 2001.

[40] T. Mogi, and S. Horiguchi, "Explosion and detonation characteristics of dimethyl ether," *J. Hazard. Mater.*, vol. 164, no. 1, pp. 114–119, 2009.

IEEE Robotics and Automation Letters (RA-L) paper, presented at ICRA 2026, Vienna, Austria. Cite as RA-L paper.

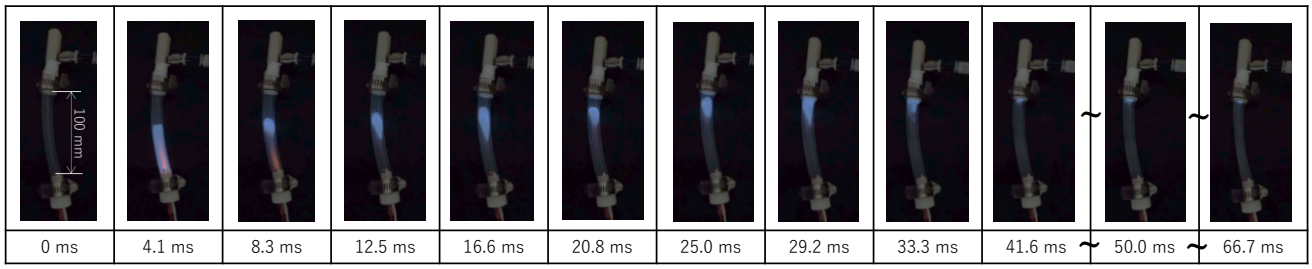

Fig. 8 Observation of flame propagation using a transparent silicone tube

TABLE III. PARAMETERS IN CHAPTER III

Q_{in}	Total amount of heat generated by combustion (Q_{in}=66.6)	*J*
Q_{dme}	Amount of heat generated per gram of DME (Q_{dme}=28.8x10^{-3})	*J*
M	Molecular weight of DME (M=46)	*g/mol*
r	Molar ratio of DME to mixed gas (r=0.07)	-
T_0	Initial temperature inside artificial muscle(T_0=299)	*K*
T_t	Temperature inside the artificial muscle after t seconds	*K*
T	Outside temperature	*K*
P_0	Initial pressure of mixed gas inside artificial muscle (P_0=0.1013)	*MPa*
P_{atm}	Atmospheric pressure	*MPa*
P_t	Pressure of the mixed gas inside the artificial muscle after t seconds	*MPa*
R	gas constant (R=8.31)	*J/mol・K*
V_0	Volume of artificial muscle (V_0=1.58x10^{-5})	m^3
d_0	Inner diameter of rubber tube （d_0=0.012）	*m*
L_0	Length of artificial muscle (L_0=0.12)	*m*
t_{dme}	Combustion time (t_{dme}=0.033)	*s*
v_{dme}	Combustion velocity of DME (v_{dme}=0)	*m/s*
q	Amount of heat per combustion time (q=2.02x10^3)	*J/s*
q_{out}	Amount of heat released from artificial muscles to the atmosphere	*J/s*
n_{dme}	Amount of DME substance (n_{dme}=5.03x10^{-5})	*mol*
c_v	Molar specific heat at constant volume of DME (c_v=12.5)	*J/mol・K*
C	Heat capacity of artificial muscle	*J/K*
S	Surface area of artificial muscle(S=5.50x10^{-3})	m^2
λ	Thermal conductivity (λ=0.25)	*W/m・K*
w_0	Thickness of artificial muscle (w_0=0.001)	*m*
n_0	Initial amount of substance inside artificial muscle(n_0=6.45x10^{-4})	*mol*
n_t	Amount of material inside artificial muscle after t seconds (n_t=6.95x10^{-4})	*mol*
F_t	Isometric contraction force of artificial muscle	*N*
θ_0	Net angle of artificial muscle	*rad*
ε_0	Contraction rate of artificial muscle (ε_0=0)	-